

****Volume Title****

*ASP Conference Series, Vol. **Volume Number***

****Author****

© ****Copyright Year**** *Astronomical Society of the Pacific*

Cosmic Ray Spectrum in Supernova Remnant Shocks

Hyesung Kang

Department of Earth Sciences, Pusan National University, Pusan 609-735, Korea

Abstract.

We performed kinetic simulations of diffusive shock acceleration in Type Ia supernova remnants (SNRs) expanding into a uniform interstellar medium (ISM). The preshock gas temperature is the primary parameter that governs the cosmic ray (CR) acceleration, while magnetic field strength and CR injection rate are secondary parameters. SNRs in the hot ISM, with an injection fraction smaller than 10^{-4} , are inefficient accelerators with less than 10 % energy getting converted to CRs. The shock structure is almost test-particle like and the ensuing CR spectrum can be steeper than E^{-2} . Although the particles can be accelerated to the knee energy of $10^{15.5}$ ZeV with amplified magnetic fields in the precursor, Alfvénic drift of scattering centers softens the source spectrum as steep as $E^{-2.1}$ and reduces the CR acceleration efficiency.

1. Introduction

Most of Galactic cosmic rays up to at least the knee energy of $10^{15.5}$ eV, are believed to be accelerated at SNRs within our Galaxy by diffusive shock acceleration (DSA) (see Hillas 2005, and references therein). In DSA theory, a small fraction of incoming thermal particles can be injected into the CR population, and accelerated to very high energies through their interactions with resonantly scattering Alfvén waves in the converging flows across the shock (Malkov & Drury 2001). Kinetic simulations of the CR acceleration at SNRs have shown that up to 50 % of explosion energy can be converted to CRs, when a fraction $10^{-4} - 10^{-3}$ of incoming thermal particles are injected into the CR population at the gas subshock (Berezhko & Völk 1997; Kang 2006). This should be enough to replenish the galactic CRs escaping from our Galaxy with $L_{CR} \sim 10^{41} \text{ erg s}^{-1}$.

Multi-band observations of nonthermal radio to γ -ray emissions from several SNRs have been successfully explained by efficient DSA features such as high degree of shock compression and the possible magnetic field amplification in the precursor (Reynolds 2008; Berezhko et al. 2009; Morlino et al. 2009). High-resolution X-ray observations of several young SNRs exhibit very thin rims, indicating the presence of magnetic fields as strong as a few $100 \mu\text{G}$ downstream of the shock (Parizot et al. 2006). Moreover, theoretical studies have shown that efficient magnetic field amplification via resonant and non-resonant wave-particle interactions is an integral part of DSA (Lucek & Bell 2000; Bell 2004). In the downstream region magnetic fields can be amplified by turbulence that is induced through cascade of vorticity generated behind curved shocks (Giacalone & Jokipii 2007). If there exist such amplified magnetic fields in the upstream region of SNRs, CR ions with charge Z might gain energies up to $E_{\text{max}} \sim$

$10^{15.5} \text{Z eV}$, which may explain the all-particle CR spectrum up to the second knee at $\sim 10^{17} \text{ eV}$ with rigidity-dependent energy cutoffs.

It has been recognized, however, that the CR spectrum at sources, $N(E) \propto E^{-s}$ with $s < 2$, predicted based on the nonlinear DSA may be too flat to be consistent with the observed flux of CR nuclei at Earth, $J(E) \propto E^{-2.7}$. Assuming an energy-dependent propagation path length ($\Lambda \propto E^{-0.6}$), a softer source spectrum with $s \sim 2.3 - 2.4$, is preferred by the observed data (*e.g.*, Ave et al. 2009). This discrepancy could be reconciled if one consider the drift of scattering centers with respect to the bulk plasma (Skilling 1975). It reduces the velocity jump that the particles experience across the shock, which in turn softens the CR spectrum beyond the canonical test-particle slope (Kang 2010; Caprioli et al. 2010; Ptuskin *et al.* 2010).

Using the spherical CRASH (Cosmic-Ray Amr SHock) code, we have calculated the CR spectrum accelerated at SNRs from Type Ia SNe expanding into a uniform interstellar medium.

2. Numerical Calculation

2.1. Spherical CRASH Code in an Expanding Grid

In the kinetic equation approach to numerical study of DSA, the following diffusion-convection equation for the particle momentum distribution, $f(r, p, t)$, is solved along with suitably modified gasdynamic equations

$$\frac{\partial g}{\partial t} + (u + u_w) \frac{\partial g}{\partial r} = \frac{1}{3r^2} \frac{\partial}{\partial r} \left[r^2 (u + u_w) \right] \left(\frac{\partial g}{\partial y} - 4g \right) + \frac{1}{r^2} \frac{\partial}{\partial r} \left[r^2 \kappa(r, y) \frac{\partial g}{\partial r} \right], \quad (1)$$

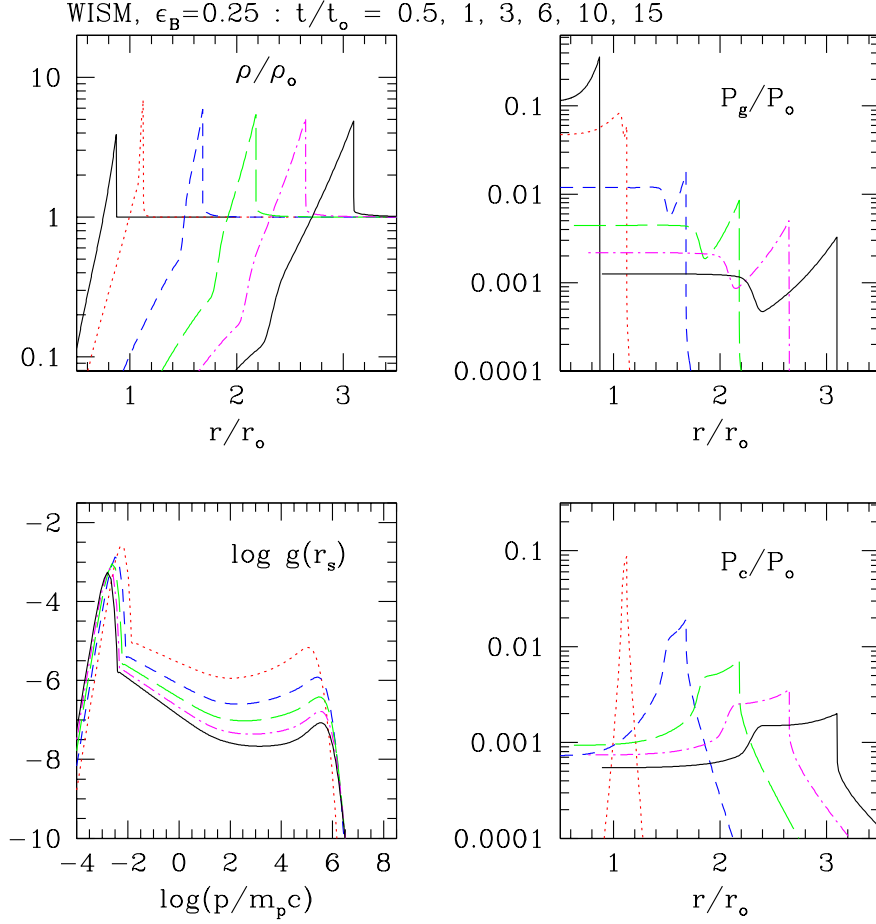
where $g = p^4 f$, with $f(p, r, t)$ the pitch angle averaged CR distribution, u_w is the wave speed, and $y = \ln(p)$, and $\kappa(r, y)$ is the diffusion coefficient parallel to the field lines (Skilling 1975).

The basic gasdynamic equations and details of the spherical CRASH code can be found in Kang & Jones (2006). The advection term of Eq. (1) is solved by the wave-propagation method, as for the gasdynamic variables, except that only the entropy wave applies. Then the diffusion term is solved by the semi-implicit Crank-Nicholson scheme. In order to implement the shock tracking and AMR (Adoptive Mesh Refinement) techniques effectively in a spherical geometry, we solve the fluid and diffusion-convection equations in a comoving frame that expands with the outer shock. Since the shock is at rest and tracked accurately as a true discontinuity, we can refine the region around the gas subshock at an arbitrarily fine level. Moreover, the shock remains at the same location in the comoving grid, so the compression rate is applied consistently to the CR distribution at the subshock. This results in much more accurate and efficient low energy CR acceleration and faster numerical convergence on coarser grid spacings, compared to the simulations in a fixed, Eulerian grid.

At quasi-parallel shocks, small anisotropy in the particle velocity distribution in the postshock fluid frame causes some particles in the high energy tail of the Maxwellian distribution to stream upstream (Giacalone *et al.* 1992; Malkov & Drury 2001). This thermal leakage injection process is treated numerically by adopting a *phenomenological* injection scheme, in which particles above a certain injection momentum p_{inj} cross the subshock and get injected to the CR population (Kang et al. 2002). One free parameter controls this process; $\epsilon_B = B_0/B_\perp$, the ratio of the general magnetic field

Table 1. Model Parameters for Supernova Remnants

Model	n_H (cm^{-3})	T_0 (K)	B_μ (μG)	r_o (pc)	t_o (years)	u_o (10^4 km s^{-1})	P_o ($10^{-6} \text{ erg cm}^{-3}$)
WISM	0.3	3.3×10^4	30	3.19	255.	1.22	1.05
MISM	0.03	10^5	30	6.87	549.	1.22	1.05×10^{-1}
HISM	0.003	10^6	5	14.8	1182.	1.22	1.05×10^{-2}

Figure 1. Time evolution of the SNR model in the warm phase ISM. The CR distribution function at the subshock, $g_s = f_s(p)p^4$, is shown as well.

along the shock normal, B_0 , to the amplitude of postshock MHD wave turbulence, B_\perp (Malkov & Völk 1998). This parameter controls the fraction of particles injected into the CR population, ξ , at the gas subshock. On the other hand, Giacalone (2005) showed that the protons can be injected efficiently even at perpendicular shocks in fully turbulent fields due to field line meandering.

Assuming that particles are resonantly scattered by self-generated waves, we adopt a Bohm-like diffusion model that represent a saturated wave spectrum, $\kappa(r, p) = \kappa_n \cdot (p/m_p c)(\rho_0/\rho)$, where $\kappa_n = m_p c^3 / (3eB_0) = 3.13 \times 10^{22} \text{ cm}^2 \text{ s}^{-1} (B_0/\mu\text{G})^{-1}$.

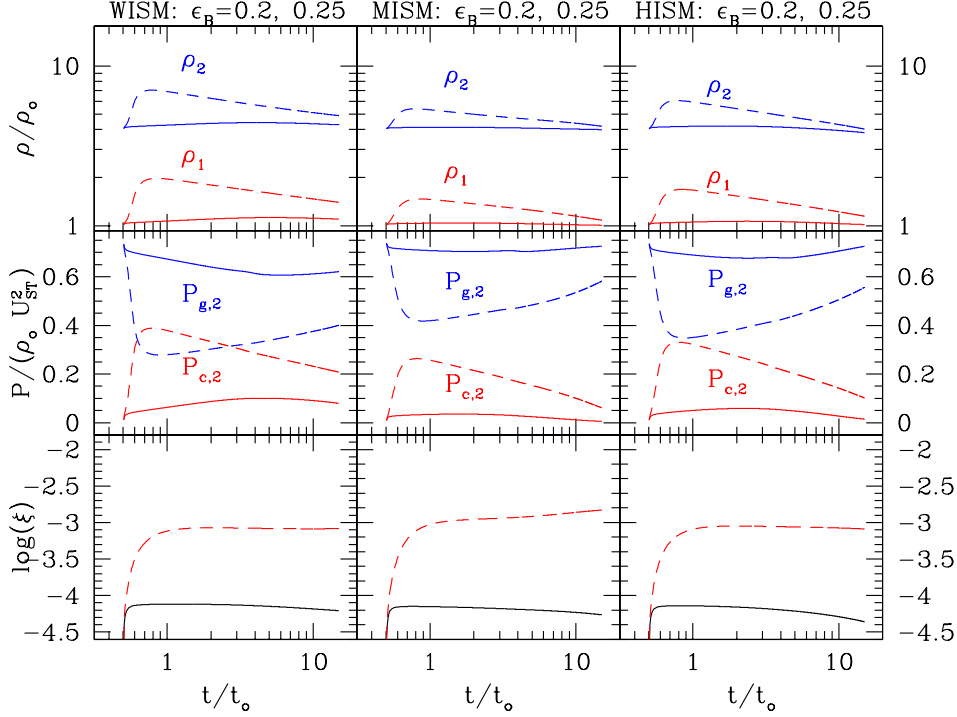


Figure 2. Immediate pre-subshock density, ρ_1 , post-subshock density, ρ_2 , post-subshock CR and gas pressure in units of the ram pressure of the unmodified Sedov-Taylor solution, $\rho_0 U_{ST}^2$, and the CR injection fraction, ξ are plotted for models WISM (left), MISM (middle), and HISM (right). Two values of $\epsilon_B = 0.20$ (solid lines) and $\epsilon_B = 0.25$ (dashed lines), are adopted.

2.2. Alfvén Wave Transport

The scattering by Alfvén waves tends to isotropize the CR distribution in the wave frame, which may drift upstream at the Alfvén speed, $u_w = v_A = B_0 / \sqrt{4\pi\rho}$, with respect to the bulk plasma flow, where B_0 is the amplified magnetic field strength (Skilling 1975). In the postshock region, $u_w = 0$ is assumed, since the Alfvénic turbulence in that region is probably relatively balanced. This Alfvénic drift reduces the velocity difference between upstream and downstream scattering centers compared to the bulk flow, leading to less efficient DSA. So the ‘modified’ test-particle slope can be estimated as $q_{tp} = 3(u_0 - v_A)/(u_0 - v_A - u_2)$, where u_2 is the downstream flow speed (Malkov & Drury 2001). Hereafter we use the subscripts ‘0’, ‘1’, and ‘2’ to denote conditions far upstream, immediately upstream and downstream of the subshock, respectively. Thus the drift of Alfvén waves in the upstream region tends to soften the CR spectrum from the canonical test-particle spectrum of $f(p) \propto p^{-4}$, if the Alfvén Mach number ($M_A = u_s/v_A$) is small.

In addition, gas heating due to Alfvén wave dissipation in the upstream region is considered by the term $W(r, t) = -v_A(\partial P_c/\partial r)$ where P_c is the CR pressure. This term is derived from a simple model in which Alfvén waves are amplified by streaming CRs and dissipated locally as heat in the precursor region. This effect reduces the subshock Mach number thereby reducing DSA efficiency (Berezhko & Völk 1997; Kang & Jones 2006).

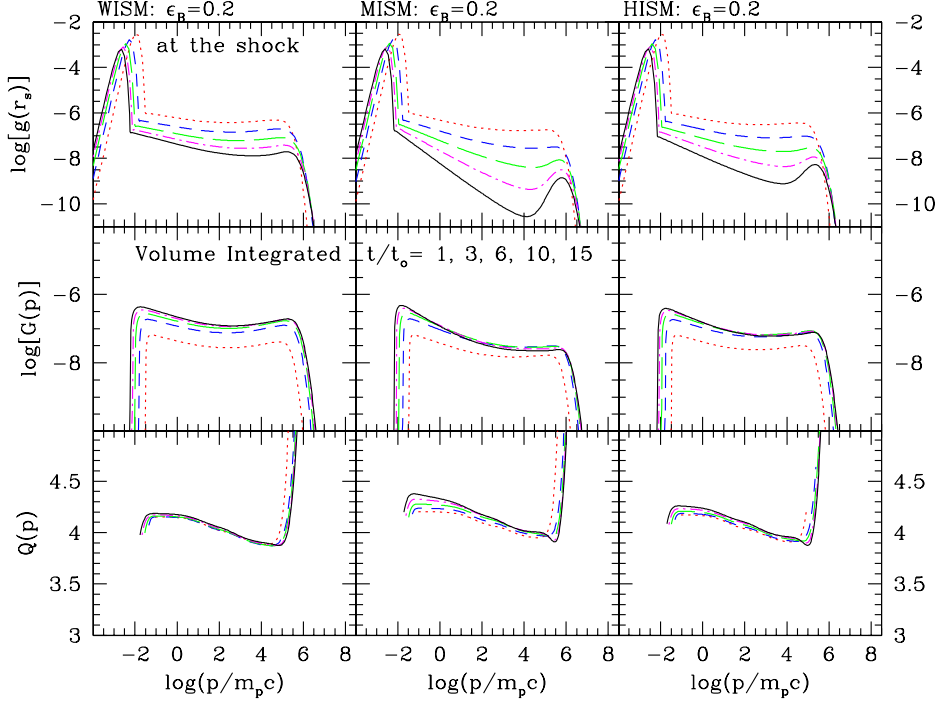


Figure 3. The CR distribution at the shock, $g(r_s, p)$, the volume integrated CR number, $G(p)$, and its slope, $Q(p)$, are shown for models with $\epsilon_B = 0.20$.

2.3. Model Parameters for Type Ia Supernova Remnants

We consider a Type Ia SN explosion with the ejecta mass, $M_{ej} = 1.4M_\odot$, expanding into a uniform ISM. All models have the explosion energy, $E_o = 10^{51}$ ergs. The shock sonic Mach number is the key parameter determining the evolution and the DSA efficiency, while the particle injection rate and magnetic field strength (through ν_A and κ_n) are secondary parameters. So here three phases of the ISM are considered: the *warm phase* with $T_0 = 3 \times 10^4$ K (WISM), the *intermediate phase* with $T_0 = 10^5$ K (MISM), and the *hot phase* with $T_0 = 10^6$ K (HISM). The presence of amplified magnetic fields a few $\times 100 \mu\text{G}$ downstream of shock has been indicated by very thin rims of several young SNRs observed in X-ray (*e.g.*, Reynolds 2008). To represent this effect we take the upstream field strength, $B_0 = 30 \mu\text{G}$ for the WISM and MISM models. For the HISM model, however, the SNR shock is much weaker and not dominated by the CR pressure, so the field amplification should be minimal. Thus the mean ISM field of $5 \mu\text{G}$ is adopted. The physical quantities are normalized by the following constants: $r_o = (3M_{ej}/4\pi\rho_o)^{1/3}$, $t_o = (\rho_o r_o^5/E_o)^{1/2}$, $u_o = r_o/t_o$, $\rho_o = (2.34 \times 10^{-24} \text{gcm}^{-3})n_H$, and $P_o = \rho_o u_o^2$. Model parameters are summarized in Table 1. Two values of $\epsilon_B = 0.20$ and $\epsilon_B = 0.25$ are adopted for inefficient and efficient injection cases, respectively.

3. Results

Figure 1 shows the time evolution of the WISM model with $\epsilon_B = 0.25$. The injection is very efficient with $\xi \approx 10^{-3}$, the shock becomes dominated by P_c and the total density

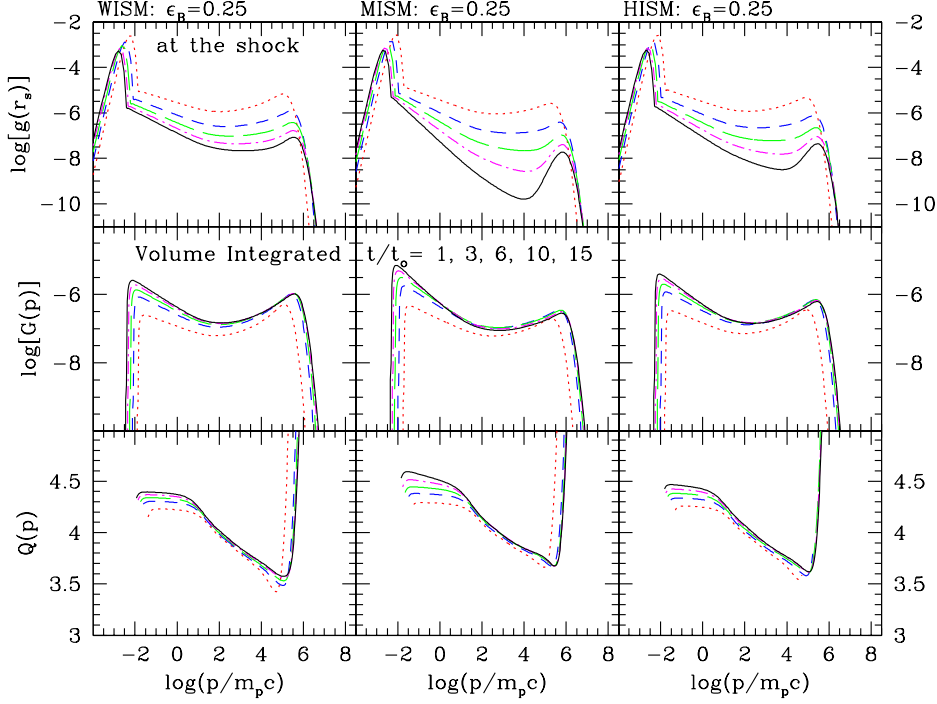


Figure 4. Same as Figure 3 except $\epsilon_B = 0.25$.

compression peaks at $\rho_2/\rho_0 \approx 6$ at $t/t_0 \sim 1$. Afterward, the CR acceleration becomes less efficient as the shock slows down and becomes weaker.

Figure 2 shows the evolution of shock properties in the different models. In the models with $\epsilon_B = 0.2$ (solid lines), the CR injection and acceleration are inefficient with the injected CR fraction, $\xi \approx 10^{-4}$, and the postshock CR pressure, $P_{c,2}/(\rho_0 U_{ST}^2) < 0.1$ through out the entire Sedov-Taylor (ST) stage. In such inefficient acceleration regime, the shock remains test-particle like with $\rho_2/\rho_0 \approx 4$ and $\rho_1/\rho_0 \approx 1$. In the models with $\epsilon_B = 0.25$ (dashed lines), on the other hand, $\xi \approx 10^{-3}$, the ratio $P_{c,2}/(\rho_0 U_{ST}^2)$ reaches up to 0.4, and the total density compression peaks at $\rho_2/\rho_0 \approx 7$. These two ratios decrease in time, since both the sonic and Alfvénic Mach numbers decrease. The WISM model is the more efficient accelerator than the HISM model, because of the higher sonic Mach number. Despite the lower sonic Mach number, in the HISM model the CR acceleration is more efficient, compared to the MISM model, because of weaker Alfvénic drift effects due to lower B_0 .

Figures 3-4 show the CR distribution function at the shock, $g(r_s, p)$, the volume integrated CR spectrum, $G(p) = \int 4\pi g(r, p) r^2 dr$, which represents the spectrum of the particles confined by the shock and its slope $Q(q) = -d \ln G / d \ln p + 4$. In all models the cutoff momentum p_{\max} approaches up to $\sim 10^{15} - 10^{15.5}$ eV/c. We note that, if the shock follows the Sedov-Taylor solution, the cutoff momentum asymptotes to $p_{\max}/m_p c \approx 0.61(u_o^2 t_o / \kappa_n) \sim 10^{6.5}$ at large t , which corresponds to $E_{\max} \approx 10^{15.5}$ eV for the WISM model. Even for the inefficient injection cases with $\xi \lesssim 10^{-4}$ the CR spectrum at the shock exhibit concave curvatures as a consequence of momentum dependent diffusion across the precursor and slowing-down of the spherical shock. Softening of the spectrum at low energies is further enhanced by the Alfvénic drift and weakening of the subshock strength in time, which is more significant in the cases of stronger

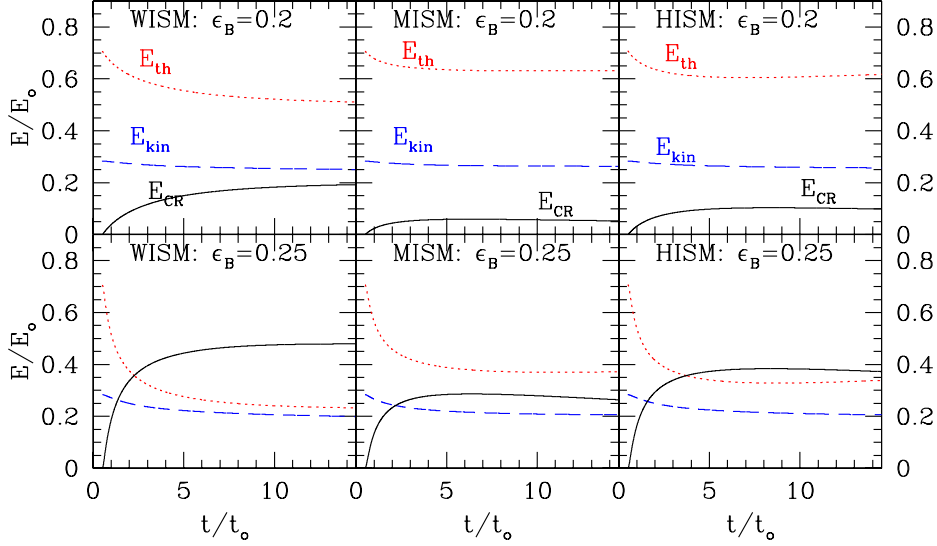


Figure 5. Total thermal, kinetic and CR energies inside the simulation volume in units of the explosion energy E_o for the models shown in Figure 2.

B_0 . However, the concavity of $G(p)$ is much less pronounced than that of $g(r_s, p)$. In the inefficient injection models, the slope, $Q(p)$, varies 4.2-4.3 at low momentum and 3.9-4.2 at high momentum, and $G(p)$ does not change significantly for $t/t_o \gtrsim 6$, especially for $10^2 m_p c < p < p_{\max}$. This implies that the acceleration is nearly balanced by the adiabatic cooling during the late stage. So we can predict that the form of $G(p)$ would remain roughly the same at much later time. In the efficient injection models with $\xi \gtrsim 10^{-3}$, of course, nonlinear feedback effects are more substantial.

Figure 5 shows the integrated energies, $E_i/E_o = 4\pi \int e_i(r) r^2 dr$, where e_{th} , e_{kin} , and e_{CR} are the densities of thermal, kinetic and cosmic ray energy, respectively. The total CR energy accelerated by $t/t_o = 15$ is $E_{CR}/E_o = 0.15, 0.05$, and 0.08 for WISM, MISM, and HISM models, respectively, for $\epsilon_B = 0.2$. These are marginally consistent with the requirement that an order of 10 % of SN explosion energy needs to be converted to CRs to replenish the Galactic CRs. In the efficient injection models with $\epsilon_B = 0.25$, the CR energy fraction approaches to $E_{CR}/E_o = 0.45, 0.25$, and 0.35 for WISM, MISM, and HISM models, respectively. The CR acceleration in the warm ISM model with $\epsilon_B = 0.25$ may be somewhat too efficient. But one has to recall that the CR injection rate may depend on the mean magnetic field direction relative to the shock surface. In a more realistic magnetic field geometry, where a uniform ISM field is swept by the spherical shock, only 10-20 % of the shock surface has a quasi-parallel field geometry (Völk et al. 2003). Moreover, Type Ia SNe make up only about 15 % of SN explosions in the Galaxy, while core collapse SNe exploding inside wind bubbles may behave differently (Hillas 2005).

4. Conclusion

In general, the DSA is very efficient for strong SNR shocks, if the injection fraction is $\xi \gtrsim 10^{-3.5}$. The CR spectrum at the subshock shows a strong concavity, not only because the shock structure is modified nonlinearly by the dominant CR pressure, but

also because the spherical SNR shock slows down in time during the Sedov-Taylor stage. Thus the concavity of the CR spectrum in SNRs is more pronounced than that in plane-parallel shocks. Moreover, the Alfvénic drift in the precursor further softens the CR spectrum as the Alfvénic Mach number decreases. However, the volume integrated spectrum, $G(p)$ (the spectrum of CRs confined by the shock including the particles in the upstream region) is much less concave. In the test-particle like solutions, $G(p)$ approaches roughly to time-asymptotic states in the late Sedov-Taylor stage, since the acceleration is nearly balanced by adiabatic cooling.

If the injection fraction is $\xi \gtrsim 10^{-3}$, about 25-45% of the explosion energy is transferred to CRs and the source CR spectrum becomes $N(E) \propto E^{-s}$ with $s \approx 1.6 - 1.8$ for $10^{11} < E < 10^{15}$ eV, which might be too flat to be consistent with the observed CR spectrum at Earth (Ave et al. 2009). If $\xi \lesssim 10^{-4}$, on the other hand, the shock structure is almost test-particle like with $\rho_2/\rho_0 \approx 4.2 - 4.4$ and the predicted source spectrum has a slope $s \approx 2.0 - 2.1$. However, the fraction of CR energy conversion, $E_{\text{CR}}/E_0 \approx 0.05 - 0.15$, might be only marginally consistent with the Galactic CR luminosity.

Finally, in all models considered in this study, for Bohm-like diffusion with the amplified magnetic field in the precursor, the particles could be accelerated to $E_{\text{max}} \approx 10^{15.5}$ ZeV. The drift and dissipation of *faster* Alfvén waves in the precursor, on the other hand, soften the CR spectrum and reduce the CR acceleration efficiency.

Acknowledgments. The author was supported by National Research Foundation of Korea through grant 2010-0016425.

References

- Ave, M., Boyle, P. J., Höppner, C., Marshall, J., & Müller, D. 2009, ApJ, 697, 106
 Bell, A.R., 2004, MNRAS, 353, 550
 Blandford, R. D. & Eichler, D. 1987, Phys. Rept., 154, 1
 Berezhko E. G., & Völk H. J. 1997, Astropart. Phys. 7, 183
 Berezhko, E. G., Ksenofontov, L. T., & Völk, H. J. 2009, A&A, 505, 169
 Caprioli, D., Blasi, P., & Amato, E., 2010, Astropart. Phys. 33, 160
 Drury, L. O’C. 1983, Rept. Prog. Phys., 46, 973
 Hillas, A. M., 2005, J. Phys. G, 31, 95
 Giacalone, J., 2005, ApJ, 628, L37
 Giacalone, J., Burgess, D., Schwartz, S. J., & Ellison, D. C. 1992, Geophys. Res. Lett., 19, 433
 Giacalone, J., & Jokipii, J. R. 2007, ApJ, 663, L41
 Kang, H. 2006, J. Korean Astronomical Society, 39, 95
 Kang, H. 2010, J. Korean Astronomical Society, 43, 25
 Kang, H., Jones, T. W., & Gieseler, U.D.J. 2002, ApJ, 579, 337
 Kang, H. & Jones, T. W., 2006, Astropart. Phys. 25, 246
 Lucek, S. G. & Bell, A. R. 2000, MNRAS, 314, 65
 Malkov, M.A. & Völk, H.J. 1998, Adv. Space Res., 21, 551
 Malkov M.A. & Drury, L. O’C. 2001, Rep. Prog. Phys., 64, 429
 Morlino, G., Amato, E., & Blasi, P. 2009, MNRAS, 392, 240
 Parizot, E., Marcowith, A., Ballet, J., & Gallant, Y. A. 2006, A&A, 453, 387
 Ptuskin, V. S., Zirakashvili, V. N., Seo, E.S. 2010, ApJ, 718, 31
 Reynolds, S. P. 2008, ARA&A, 46, 89
 Skilling, J. 1975, MNRAS, 172, 557
 Völk, H. J., Berezhko, E. G., & Ksenofontov, L. T. 2003, A&A, 409, 563